10

Distribution of NBOHC color centers in birefringent microtracks induced by laser radiation in the bulk of fused silica

© A.E. Rupasov, G.K. Krasin, Y.S. Gulina, I.D. Matyaev, S.I. Kudryashov

P.N. Lebedev Physical Institute, Russian Academy of Sciences, Moscow, Russia

e-mail: rupasovan@lebedev.ru

Received February 07, 2025
Revised March 28, 2025
Accepted June 02, 2025

This study presents the first investigation of the distribution of non-bridging oxygen hole centers (NBOHCs) within birefringent microtracks in fused silica and correlates it with their spatial structure. A photoluminescence band peaking at 650 nm, associated with NBOHC formation, was identified, and the dependence of its integrated intensity on the longitudinal coordinate along the microtrack was determined. Micron-scale structure in the microtrack cross-section was detected via photoluminescence signals from these centers. The dependence of microtrack birefringence magnitude ($\Delta n \sim 10^{-3}$) on laser pulse energy density was established. Mechanisms of fused silica modification were determined using Raman spectroscopy.

Keywords: Direct laser writing, femtosecond laser pulses, silica, nanogratings.

DOI: 10.61011/EOS.2025.06.61666.7595-25

Introduction

Currently, the technology of laser writing microtracks inside transparent solid dielectrics using ultrashort pulses is actively being studied and developed. The distinctive feature of such microtracks is the birefringence effect. Birefringent microtracks represent stable changes in the material that form along the radiation propagation axis [1]. This effect is due to the presence of an ordered submicron substructure with a period smaller than the wavelength of the inducing laser radiation [2–5]. The substructure consists of regions of material densification and rarefaction, accompanied by the formation of color centers [6,7].

The method of laser writing birefringent microstructures underlies the development of optical memory [8–10], the creation of optical elements such as polarization components [11], wave phase plates [12], microfilters [13], and photonic components and devices [14–17]. However, when forming birefringent microstructures in fused silica, a problem arises — the appearance of color centers, which reduces the transparency of the resulting structure [18]. This significantly limits the possibilities for practical application of these technologies.

In this work, a study was conducted on the distribution of non-bridging oxygen hole centers (NBOHCs) along birefringent microtracks depending on the energy density of the inducing laser radiation. The obtained results were compared with the subwavelength substructure of microtracks visualized using scanning electron microscopy. Photoluminescence of NBOHC centers revealed the presence of a micron-scale structure along the wave vector of the inducing radiation.

Experiment

The experimental setup (Fig. 1), used for recording birefringent structures, is based on the Satsuma laser system. Its core is a fiber ytterbium laser with a wavelength of 1030 nm. In the experiment, laser radiation was focused using a microscope objective with a numerical aperture NA = 0.45 into a focal spot with an energy level radius of $1/e^2$ approximately $w_0 \sim 2\,\mu$m and a Rayleigh length $Z_R \approx 12\,\mu$m.

The radiation was focused inside a fused silica sample at a depth of 100 μm. The sample had the shape of a parallelepiped with dimensions $20 \times 10 \times 2\,\text{mm}^3$ and was mounted on a three-axis motorized platform. The experiment was conducted with the following parameters: pulse repetition rate — 100 kHz, sample translation speed 300 μm/s. Pulse durations were 0.3 and 0.6 ps, with energy ranging from 0.1 to 3 μJ.

Analysis of birefringence characteristics in the recorded regions was performed using a Thorlabs polarimetry system

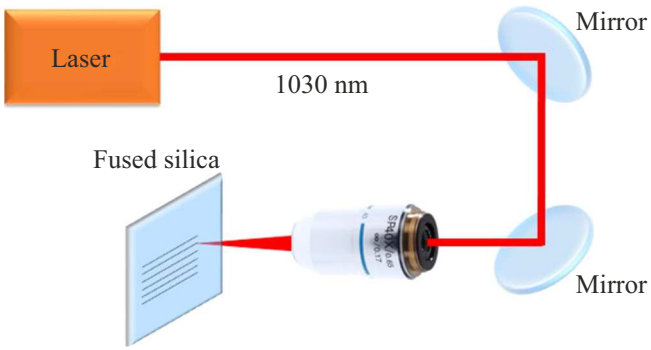

Figure 1. Diagram of the experimental setup.

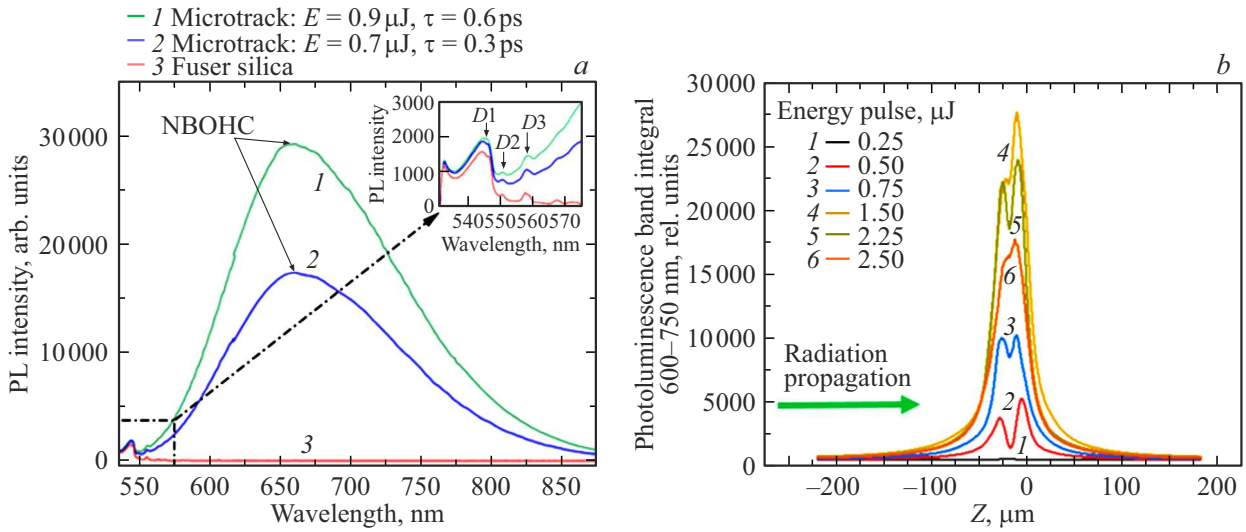

Figure 2. (*a*) Photoluminescence and Raman scattering spectra of birefringent microtracks in fused silica ($\Lambda = 1030$ nm, 100 kHz, $\tau = 0.3$ ps). (*b*) Dependence of the integral of the 600–750 nm photoluminescence spectrum band on the coordinate along the microtrack.

operating at a wavelength of 633 nm [19]. To compare the birefringence parameters with the formed substructure of microtracks, structural studies were conducted.

A sample with recorded regions of birefringent microtracks was cut across to visualize the microtracks in cross-section. For this purpose, a diamond dicing saw DAD 3220 (DISCO) was used, followed by polishing on a PM5 machine (Logitech) using corundum abrasives of size 3–10 μm and silicon oxide nanoparticles of size 25 nm.

Visualization of microtracks was performed using a Tescan Vega 3 scanning electron microscope. A confocal laser scanning microscope with a 532 nm laser source was used to study photoluminescence and Raman scattering.

Results

Photoluminescence spectra were recorded in the region of birefringent microtrack formation, written with pulses of duration 0.3 and 0.6 ps and energies 0.7 and 0.9 μJ respectively, under excitation by a laser at a wavelength of 532 nm (Fig. 2, *a*). The inset shows an enlarged fragment of the spectrum with characteristic Raman scattering peaks for fused silica $D1$ (495 cm^{-1}, 546 nm), $D2$ (606 cm^{-1}, 549 nm) and $D3$ (805 cm^{-1}, 556 nm), corresponding to bridging Si-O-Si bonds. Relative intensities of the RS peaks reflect densification or rarefaction of fused silica [20]. As seen from the photoluminescence graphs in the modified and unmodified regions, in the region of birefringent microtrack formation, the photoluminescence signal intensity at a wavelength of 650 nm increases, and the intensity for longer pulses is almost twice as high despite nearly identical energy (Fig. 2, *a*). This may be related to the formation of non-bridging oxygen hole centers (=Si-O′, NBOHC) — laser-induced color centers [6,7].

To correlate the spatial substructure of the birefringent microtrack with the induced refractive index difference, the dependence of the integral of the 600–750 nm photoluminescence band on the coordinate along the microtrack was obtained (Fig. 2, *a*). The selection of this spectral range was determined by the diffraction grating used in the spectrometer. From the graphs of luminescence signal integral versus coordinate, it can be estimated how structural modification (formation of NBOHC color centers) occurs along the birefringent microtrack, which, in turn, is responsible for inducing the anisotropic effect, i.e., birefringence. Thus, with increasing pulse energy of the inducing radiation, the redistribution of color center photoluminescence intensity along the microtrack occurs, with NBOHC color centers distributed non-uniformly along the microtrack.

Visualization of microtrack cross-sections was performed using scanning electron microscopy (SEM) and confocal laser scanning microscopy. Images obtained by SEM demonstrate the presence of a submicron substructure of birefringent microtracks with periods along the wave vector Λ_k and along the electric field vector Λ_E of the inducing laser radiation. Confocal microscopy allows identification of color center distribution in microtracks. For microtracks, the signal maximum corresponds to the pre-focal region, and as the distance from the focal plane increases, the intensity of color center photoluminescence decreases, which is related to the formation of a complex longitudinal-transverse spatial subwavelength substructure along the microtrack (Fig. 3, *a*).

Within the study, the relationship between photoluminescence intensity $S = \int_0^L I_{pl}(l)dl$ and birefringence magnitude $\Delta n = \Gamma/L$, was investigated, where Γ — is the optical path difference recalculated from the phase shift. An estimate of microtrack length L depending on laser pulse energy density was performed using the photoluminescence signal at half maximum from the coordinate (Fig. 2, *b*). It was found that

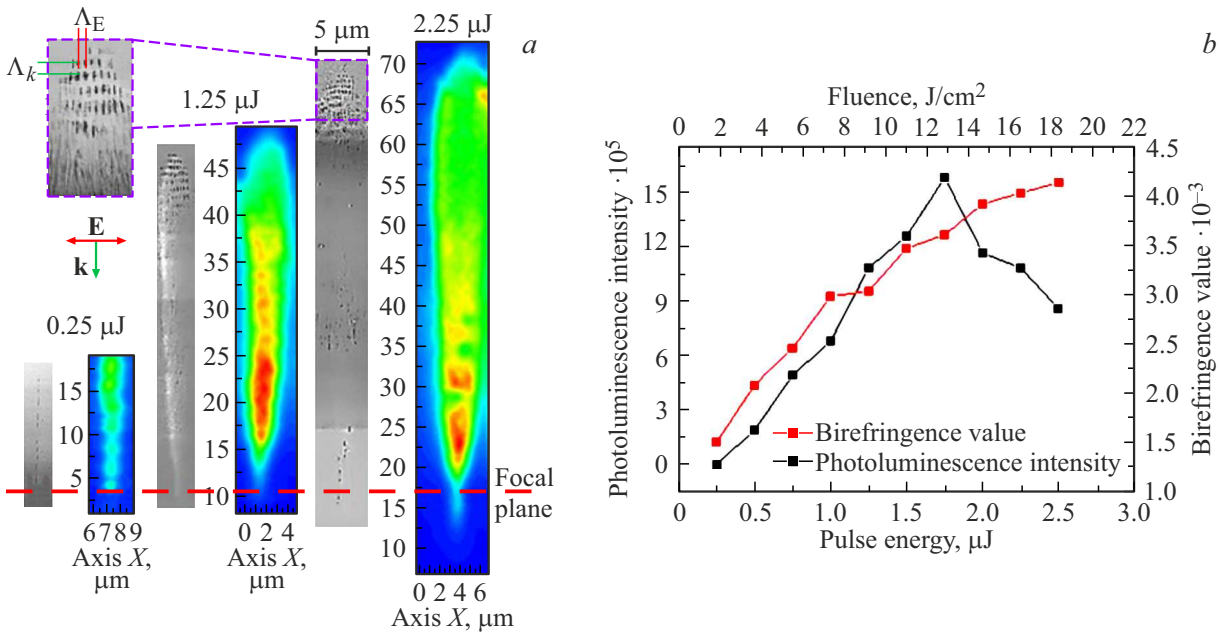

Figure 3. (*a*) Maps of microtrack cross-sections reflecting the distribution of NBOHC center photoluminescence under 532 nm laser excitation, and SEM images of microtrack cross-sections. (*b*) Dependence of photoluminescence intensity and birefringence magnitude on the threshold pulse energy density.

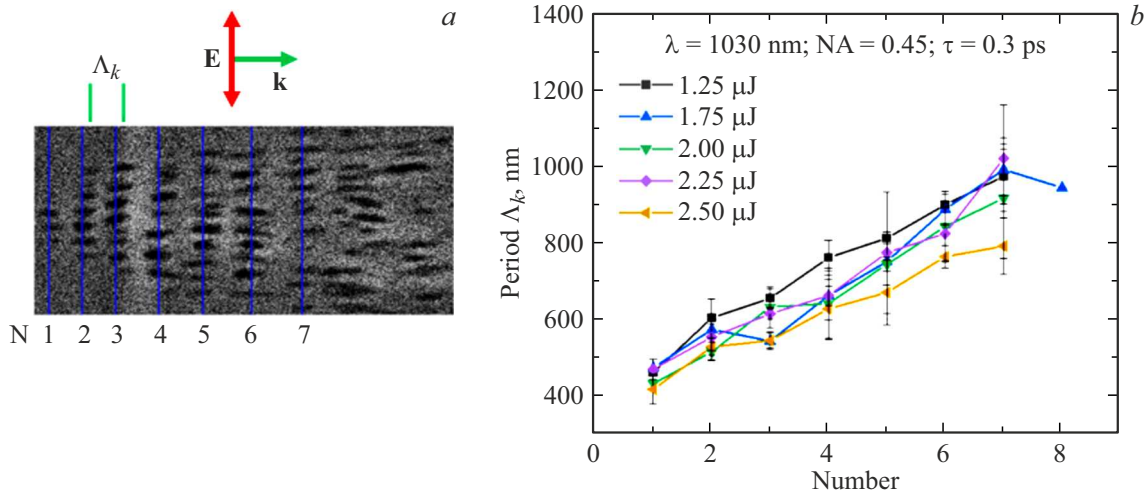

Figure 4. (*a*) SEM image of the microtrack substructure along the wave vector. (*b*) Dependence of the microtrack period magnitude Λ_k on the period number for different pulse energies.

exceeding the threshold energy density of 15 μJ/cm^2 leads to a decrease in photoluminescence intensity (Fig. 3, *b*). This indicates that increasing energy density beyond a certain threshold reduces NBOHC color center photoluminescence intensity. Additionally, it was established that birefringence magnitude smoothly increases with rising threshold energy density of the pulse inducing birefringent structures. This result suggests that increasing energy density leads to more pronounced birefringent structures.

Periods of microtrack substructure along the wave vectorΛ_k (Fig. 4) and along the electric field vector Λ_E (Fig. 5) were analyzed depending on pulse energy [21]. During the study, it was revealed that the period of birefringent microtracks oriented along the wave vector is not constant. This observation may be associated with non-uniform plasma density distribution in the material, which contributes negatively to the permittivity [22,23]. Notably, the periods discovered practically do not depend on pulse energy and fall within the submicron range. This indicates that microtrack formation and properties are determined not only by laser pulse energy but also by other factors such as plasma density distribution and material properties.

Pseudocolor maps of NBOHC color center photoluminescence integral in the 600–750 nm band were obtained,

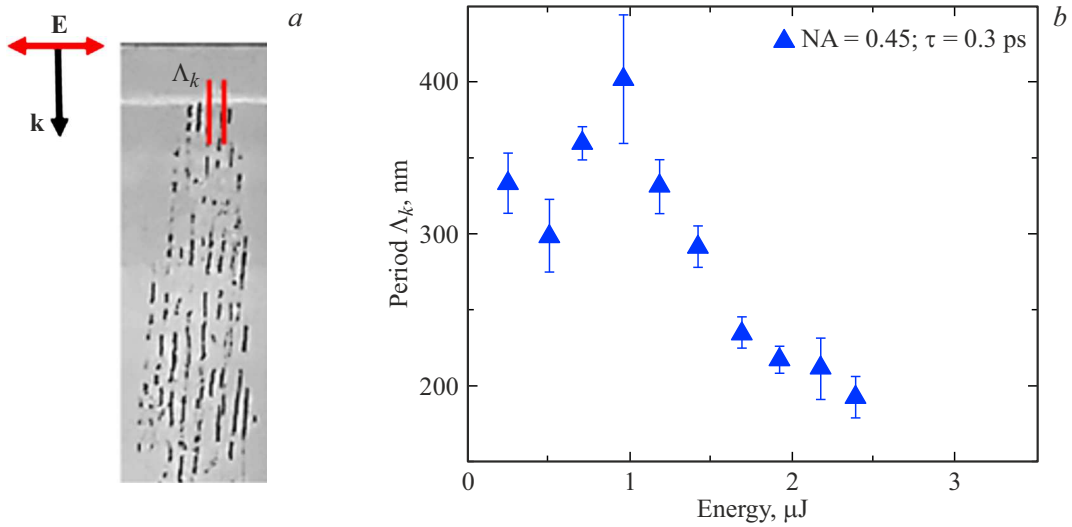

Figure 5. (*a*) SEM image of the microtrack substructure along the electric field vector. (*b*) Dependence of the microtrack period magnitude Λ_E on pulse energy.

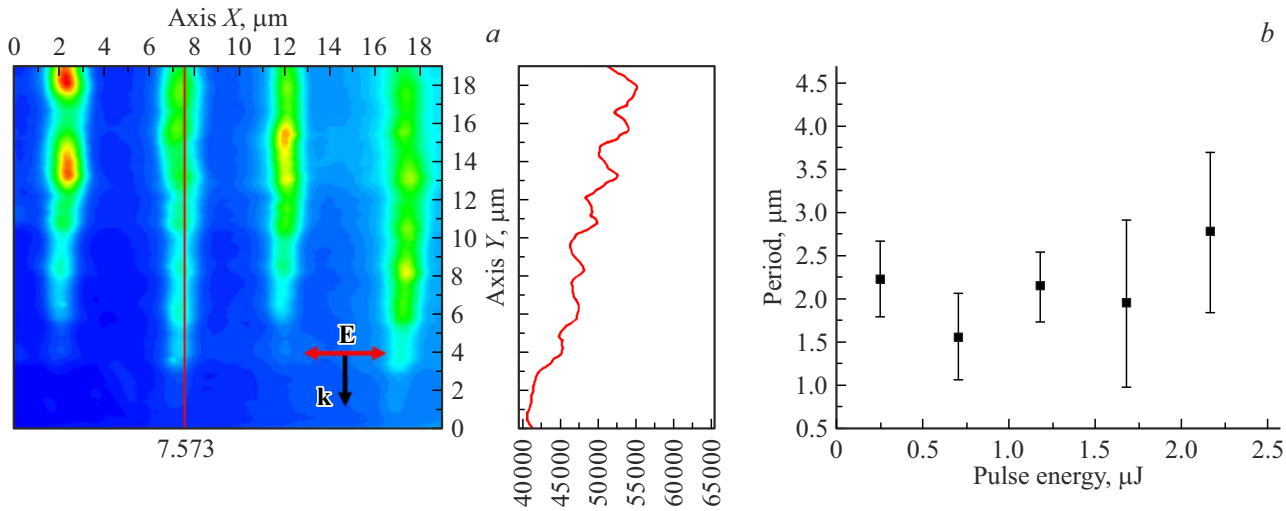

Figure 6. (*a*) Photoluminescent microtrack profile: graphical representation where each point is the integral of the photoluminescence band in the 600–750 nm range. (*b*) Dependence of photoluminescence periods on pulse energy.

where micron-scale periods are observed along the wave vector (Fig. 6). When visualized using scanning electron microscopy, the period of structures is less than a micron and falls into the submicron range. Visualization of birefringent microtracks in cross-section via confocal microscopy yields a structure with micron-scale periods along the wave vector direction.

This effect cannot be associated with self-focusing and defocusing along laser radiation propagation in fused silica, previously interpreted by the moving foci model [24,25], when exceeding critical self-focusing power ($P > P_{cr}$) [26]. For fused silica under our conditions, its value calculated from expression $P_{cr} = 3.77 \times \lambda^2/(8\pi n_0 n_2)$ [24,25] is 2.8 MW. The periodic structure forms along radiation propagation at power below critical self-focusing powers; the minimum power value was 0.83 MW, though it should be noted that self-focusing theories for tightly focused pulses have not yet been developed, and the equation for critical self-focusing power does not account for numerical aperture influence [27]. In lithium niobate, supercritical electron-hole plasma in filaments was observed earlier. It causes excitation of plasmon-polaritons at the boundary with unexcited dielectric, leading to nanoplasmonic modulation of plasma density. Corresponding material Bragg gratings were imprinted in crystalline lithium niobate [28].

Conclusion

Within the study, the distribution of NBOHC color centers inside microtracks was investigated for the first

time. In the region of birefringent microtrack formation, a photoluminescence band with a peak at 650 nm was identified, associated with non-bridging oxygen hole centers (=Si-O′, NBOHC). The spatial structure of birefringent microtracks recorded inside fused silica under tight focusing with ultrashort laser pulses of wavelength 1030 nm and durations 0.3 and 0.6 ps at variable pulse energies was compared. As a result, the dependence of the photoluminescence spectrum integral on the coordinate along the microtrack was obtained, reflecting structural changes along it. Additionally, a micron-scale structure along the wave vector was discovered when visualizing NBOHC color centers in microtrack cross-sections, formed below critical self-focusing power. The dependence of microtrack birefringence magnitude on pulse energy density, on the order of $\Delta n \sim 10^{-3}$ was determined. Physical mechanisms of fused silica modification in the region of birefringent microtrack formation and their subwavelength substructure were established from Raman scattering spectra, revealing transformations of peaks $D1$ ($495\,cm^{-1}$, 546 nm), $D2$ ($606\,cm^{-1}$, 549 nm) and $D3$ ($805\,cm^{-1}$, 556 nm) corresponding to bridging bonds. Si-O-Si.

Funding

The study was supported by a grant provided by the Russian Science Foundation (Project № 22-72-10076).

Conflict of interest

The authors declare that they have no conflict of interest.

References

[1] E. Bricchi, B.G. Klappauf, P.G. Kazansky. Opt. Lett., **29** (1), 119 (2004). DOI: 10.1364/ol.29.000119
[2] Y. Shimotsuma, P.G. Kazansky, J. Qiu, K. Hirao, Phys. Rev. Lett., **91** (24), 247405 (2003). DOI: 10.1103/physrevlett.91.247405
[3] R. Taylor, C. Hnatovsky, E. Simova. Laser Photonics Rev., **2** (1−2), 26 (2008). DOI: 10.1002/lpor.200710031
[4] W. Yang, E. Bricchi, P.G. Kazansky. J. Bovatsek, A.Y. Arai. Opt. Exp., **14** (21), 10117 (2006). DOI: 10.1364/oe.14.010117
[5] V.R. Bhardwaj, E. Simova, P.P. Rajeev, C. Hnatovsky, R.S. Taylor, D.M. Rayner, P.B. Corkum. Phys. Rev. Lett., **96** (5), 057404 (2006). DOI: 10.1103/physrevlett.96.057404
[6] H.B. Sun, S. Juodkazis, M. Watanabe, S. Matsuo, H. Misawa, J. Nishii. J. Phys. Chem. B, **104** (15), 3450 (2000). DOI: 10.1021/jp992828h
[7] K. Mishchik, C. d'Amico, P.K. Velpula, C. Mauclair, A. Boukenter, Y. Ouerdane, R. Stoian. J. Appl. Phys., 114(13), 133502(2013). DOI: 10.1063/1.4822313
[8] H. Wang, Y. Lei, L. Wang, M. Sakakura, Y. Yu, G. Shayeganrad, P.G. Kazansky. Laser Photonics Rev., **16** (4), 2100563 (2022). DOI: 10.1002/lpor.202100563
[9] Z. Wang, B. Zhang, Z. Wang, J. Zhang, P.G. Kazansky, D. Tan, J. Qiu. Adv. Mater., **35** (47), 2370344(2023). DOI: 10.1002/adma.202303256
[10] J. Gao, X.J. Zhao, Z. Yan, Y. Fu, J. Qiu, L. Wang, J. Zhang. Adv. Func. Mater., **34** (11), 2306870 (2024). DOI: 10.1002/adfm.202306870
[11] Y. Shimotsuma, M. Sakakura, P.G. Kazansky, M. Beresna, J. Qiu, K. Miura, K. Hirao. Adv. Mater., **22** (36), 4039(2010). DOI: 10.1002/adma.201000921
[12] M. Beresna, M. Gecevičius, P.G. Kazansky, T. Gertus. Appl. Phys. Lett., **98** (20), 562 (2011). DOI: 10.1063/1.3590716
[13] S.I. Kudryashov, P.A. Danilov, A.E. Rupasov, M.P. Smayev, N.A. Smirnov, V.V. Kesaev, S.A. Gonchukov. Laser Phys. Lett, **19** (6), 065602(2022). DOI: 10.1088/1612-202X/ac6806.
[14] J.D. Mills, P.G. Kazansky, E. Bricchi, J.J. Baumberg. Appl. Phys. Lett., **81** (2), 196 (2002). DOI: 10.1063/1.1492004
[15] F. Flamini, L. Magrini, A.S. Rab, N. Spagnolo, V. D'ambrosio, P. Mataloni, R. Osellame. Light Sci. Appl., **4** (11), e354(2015). DOI: 10.1038/lsa.2015.127
[16] R. Osellame, H.J. Hoekstra, G. Cerullo, M. Pollnau. Laser & Photon. Rev., **5** (3), 442(2011). DOI: 10.1002/lpor.201000031
[17] R. Stoian, C. D'amico, Y. Bellouard, G. Cheng. *Ultrafast Laser Nanostructuring: The Pursuit of Extreme Scales*. (Springer International Publishing, Cham, 2023), p. 1053. DOI: 10.1007/978-3-031-14752-4
[18] G. Shayeganrad, X. Chang, H. Wang, C. Deng, Y. Lei, P.G. Kazansky. Opt. Exp., **30** (22), 41002(2022). DOI: 10.1364/oe.473469
[19] S.B. Mehta, M. Shribak, R. Oldenbourg. J. Opt., **15** (9), 094007(2013). DOI: 10.1088/2040- 8978/15/9/094007
[20] J. Burgin, C. Guillon, P. Langot, F. Vallée, B. Hehlen, M. Foret. Phys. Rev. B, **78** (18), 184203(2008). DOI: 10.1103/physrevb.78.184203
[21] Yu.S. Gulina, A.E. Rupasov, G.K. Krasin, N.I. Busleev, I.V. gritsenko, A.V. Bogatskaya, S.I. Kudryashov. Pisma v ZhETF, **119** (9), 638 (2024) (in Russian). DOI: 10.31857/S1234567824090027
[22] A. Couairon, L. Sudrie, M. Franco, B. Prade, A. Mysyrowicz (2005). Phys. Rev. B, **71** (12), 125435(2005). DOI: 10.1103/physrevb.71.125435
[23] A. Couairon, A. Mysyrowicz. Phys. Rep., **441** (2−4), 47(2007). DOI: 10.1016/j.physrep.2006.12.005
[24] N. I. Lipatov, A. A. Manenkov, A. M. Prokhorov. Pisma v ZhETF **11**, 444 (1970) (in Russian).
[25] S. Tzortzakis, L. Sudrie, M. Franco, B. Prade, A. Mysyrowicz, A. Couairon, L. Bergé. Phys. Rev. Lett., **87** (21), 213902(2001). DOI: 10.1103/PhysRevLett.87.213902
[26] S.I. Kudryashov, P.A. Danilov, E.V. Kuzmin, Y.S. Gulina, A.E. Rupasov, G.K. Krasin, A.A. Ionin. Opt. Lett., **47** (14), 3487(2022). DOI: 10.1364/ol.462693
[27] B. G. Gorshkov. *Metod MBR v kvantovoi elektronike i lazernoe razrushenie. (in Russian) Trudy FIAN* (Nauka, M., 1982), p. 81.
[28] S. Kudryashov, P. Danilov, A. Gorevoy, V. Kovalov, M. Kosobokov, A. Akhmatkhanov, V. Shur. Photon., **10** (12), 1316(2023). DOI: 10.3390/photonics10121316

Translated by J.Savelyeva